1 # Title: Atomic model of microtubule-bound tau

2

3

4 **Authors:** Elizabeth H. Kellogg[1,2,*], Nisreen M.A Hejab[2,*], Simon Poepsel[1], Kenneth H.

5 Downing[2], Frank DiMaio[3,4] and Eva Nogales[1,2,5,#]

6

7 **Affiliations:**

8 * These authors contributed equally to this work

9 [1] QB3 Institute and Molecular and Cell Biology Department, UC Berkeley, CA 94720-

10 3220

11 [2] Molecular Biophysics and Integrated Bioimaging Division, Lawrence Berkeley National

12 Laboratory, CA 94720

13 [3] Department of Biochemistry University of Washington, Seattle, WA 98195-7370

14 [4] Institute for Protein Design, Seattle, WA, 98195-1655

15

16 [5] Howard Hughes Medical Institute, UC Berkeley, CA 94720-322

17 # Corresponding author (enogales@lbl.gov)

18 **One Sentence Summary:** Using cryo-EM and atomic modeling, we present an atomic

19 model of microtubule-bound tau that is consistent with prior biochemical studies and

20 provides an explanation for disease-associated phosphorylation data.

21

1

22

23 **Abstract:**

24 Tau is a developmentally regulated protein found in axons, whose physiological role is

25 to stabilize and bundle microtubules (MTs). Hyper-phosphorylation of tau is thought to

26 cause its detachment from MTs and subsequent aggregation into pathological fibrils that

27 have been implicated in Alzheimer's disease pathogenesis. Despite its known MT

28 binding role, there is no consensus regarding which tau residues are crucial for tau-MT

29 interactions, where on the MT tau binds, and how binding results in MT stabilization. We

30 have used cryo-EM to visualize the interaction of different tau constructs with MTs at

31 high resolution (3.2-4.8 Å) and used computational approaches to generate atomic

32 models of tau-tubulin interactions. Our work shows that the highly conserved tubulin-

33 binding repeats within tau adopt very similar structures in their interactions with the MT.

34 Each tau repeat binds the MT exterior and adopts an extended structure along the crest

35 of the protofilament (PF), interacting with both α- and β-tubulin, thus stabilizing the

36 interface between tubulin dimers. Our structures agree with and explain previous

37 biochemical data concerning the effect of phosphorylation on MT affinity and lead to a

38 model in which tau repeats bind in tandem along a PF, tethering together tubulin dimers

39 and stabilizing longitudinal polymerization interfaces. These structural findings could

40 establish a basis of future treatments aiming at the selective stabilization of tau-MT

41 interactions.

42

43

Main Text

44

45   The microtubule (MT) cytoskeleton is essential for many eukaryotic cellular functions,

46   including cellular trafficking and chromosome segregation. MTs are formed by the head-to-tail

47   assembly of $\alpha\beta$-tubulin dimers into protofilaments (PFs), which in turn associate laterally to form

48   hollow tubes. The properties and cellular functions of MTs are regulated by their interaction with

49   a myriad of MT associated proteins (MAPs). In neurons, MTs interact with a family of "classical"

50   MAPs, including MAP-2, MAP-4, and tau, that contribute to MT organization and stability and

51   are critical to neuronal growth and function. Tau, which constitutes more than 80% of neuronal

52   MAPs, localizes to axons where it functions to stabilize and bundle MTs(*1*) and is

53   developmentally regulated(*2*).

54   Tau and its homologs are intrinsically disordered proteins containing an array of

55   conserved MT-binding sequences. Full-length tau from adult human neurons(*3*) includes a

56   projection domain, a central, MT-binding region containing four imperfect sequence repeats, R1-

57   4, and a C-terminal domain (Fig. 1A). Different MT binding repeats have been shown to bind to

58   and stabilize MTs(*4, 5*), with the affinity and MT stabilization activity increasing with the number

59   of repeats(*5, 6*). Neurodegenerative disorders known as tauopathies, including Alzheimer's

60   disease, develop when tau is abnormally phosphorylated and its affinity for MTs is reduced(*7-9*).

61   Dissociation from MTs ultimately leads to the formation of intracellular, filamentous tau

62   aggregates, called neurofibrillary tangles.

63   While the high-resolution structure of the amyloid tau aggregates has recently been

64   described(*10*), the physiologically relevant conformation of MT-bound tau is still poorly

65   understood. NMR and fluorescence spectroscopy data indicated that the MT-binding domain of

66   tau could adopt a helical structure upon association with MTs(*11, 12*), while solid-state NMR

67   studies suggested a structured hairpin conformation(*13*). Cryo-electron microscopy (cryo-EM)

68   studies also resulted in contradictory proposals concerning the tau binding site on MTs. While

69   tau was reported to bind along PFs when added to pre-formed, Taxol-stabilized MTs(*14*), it was

3

70   proposed to bind near the Taxol-binding site on the luminal MT surface if tubulin was co-

71   polymerized with tau in the absence of the drug(*15*). The low resolution attainable at the time of

72   these reports added to the uncertainty of their conclusions. Defining the high-resolution

73   structure of MT-bound tau has implications for Alzheimer's treatment through a better

74   understanding of how tau phosphorylation and mutations contribute to loss of native function

75   and onset of disease. Here, we present atomic structures of MT-bound tau using a hybrid

76   approach that combines state-of-the-art cryo-EM imaging with computational protein structure

77   determination.

78

79   In order to visualize tau on MTs, we first assembled dynamic MTs in the presence of

80   excess full-length tau, and carried out cryo-EM studies following our previously established

81   protocols to obtain high-resolution MT structures(*16-18*). The cryo-EM reconstruction (overall

82   resolution of 4.1 Å (Fig. S1C)) shows tau as a narrow, discontinuous density along each PF

83   (Fig. 1B), approximately following the outermost ridge on the MT surface defined by the H11-

84   H12 helices of both α- and β-tubulin. The tau density is adjacent to the site of attachment of the

85   unstructured C-terminal tails (Fig. 1C), in agreement with biochemical data highlighting the

86   importance of the acidic tails of tubulin for tau affinity(*19, 20*). This location is fully consistent with

87   the previous cryo-EM reconstruction by Al-Bassam and Milligan(*14*), but the higher resolution

88   now allows us to conclude that the density correspond to a fully extended chain, rather than an

89   α-helical segment, as previously proposed. To probe for the existence of a tau-MT binding site

90   within the MT interior, we added tau either to pre-formed MTs or to polymerizing tubulin, both in

91   the absence of Taxol (see Methods). None of the reconstructions showed any tau density on the

92   MT luminal surface (data not shown). Thus, contrary to a previous report(*15*), we identified a

93   single binding site on the MT exterior regardless of preparation conditions.

94

95   In addition to full-length tau, we also examined two N- and C-terminally truncated tau constructs

96   that included either all four repeats (4Repeat) or just the first two repeat sequences (2Repeat)

97   (Fig. S1A and B, respectively). The 4Repeat- and 2Repeat-MT cryo-EM reconstructions are

98   indistinguishable from the full-length tau at the present resolution (estimated overall resolutions

99   of 4.8 Å and 5.6 Å, respectively (Fig. S1C)). In all three cases the length of the density ascribed

100   to tau corresponds to an extended chain of about 27 aa (see later), with a connecting region of

101   very weak density that would accommodate another 3-4 extended residues, thus adding up to

102   the length of the tau repeats (31 aa). This finding strongly suggests that each segment of the

103   observed density is attributable to a single repeat. The fact that the 2Repeat, 4Repeat, and full-

104   length tau reconstructions are basically indistinguishable indicates that the repeats likely adopt

105   similar structures on the MT-surface upon binding. It is important to note that, given the nature

106   of our reconstruction procedures (see Methods), the cryo-EM structures for these tau constructs

107   correspond to an average of the different repeats.

108

109   The resolution for the tau density within these reconstructions (4.6-6.5 Å) is significantly

110   lower than that for tubulin (4 to 4.5 Å) (Fig. S2), which could be due to sub-stoichiometric

111   binding, flexibility, compositional heterogeneity (i.e. sequence differences between the repeats),

112   or a combination of these factors. Thus, we decided to pursue the structure of a synthetic tau

113   construct comprising four identical copies of R1 (R1x4) (Fig. 2). The cryo-EM reconstruction of

114   the R1x4-MT reached an overall resolution of 3.2 Å (Fig. 2A, Fig. S1C), with local resolution for

115   tau ranging from 3.7 Å to 4.2 Å (Fig. S2). Again, tau appears as regularly spaced segments

116   separated by fragments of more discontinuous density. Consistent with conclusions from

117   previous studies(*5, 21*), the alternation of well-defined and weaker tau density indicates that tau

118   has tightly-bound segments interspersed with more mobile regions. We built a poly-alanine

119   model into the best-resolved segment of the R1x4 tau density, at the inter-dimer interface, that

120   accommodated 12 residues. Prior studies showed that tau fragments as small as 18 amino

121   acids were sufficient to promote MT polymerization and stabilization(*4*). The tau binding site

122   partly overlaps with that of the motor domain of kinesin (Fig. S3), consistent with reports that tau

123   binding interferes with kinesin-MT attachment(*22*).

124

125   Due to the lack of unambiguously identifiable large sidechains and the absence of

126   regular secondary structure, obtaining the correct sequence register for tau proved challenging.

127   Therefore, we used Rosetta(*23*) as an unbiased approach to simultaneously assess the

128   energetics and density-agreement of potential tau sequence registers (see Methods). We

129   identified a single register and conformation that was significantly favored, both energetically

130   and based on fit to density, and that included aa 256-267 (VKSKIGSTENLK) (Fig. 2B). An

131   alternative refinement protocol(*24*) allowing further conformational sampling converged to the

132   same amino acid sequence and structure (Fig. S4). The modeled segment corresponds to a

133   conserved 12 aa sequence motif that lies within the 18 aa fragment previously shown to be

134   sufficient to promote MT polymerization *in vitro*(*4, 25*). In the proposed atomic model, conserved

135   residues play critical roles in MT-tau interactions (Fig. 2C). Ser258 and Ser262 form hydrogen

136   bonds with α-tubulin Glu434. Importantly, phosphorylation of the universally conserved Ser262

137   (Fig. S5) has been previously shown to strongly attenuate tau-MT binding(*26*) and is a marker of

138   Alzheimer's disease(*27*). Though Thr263 is also positioned to hydrogen-bond with Glu434,

139   hydrophobic substitutions are tolerated at this position (Fig. S5), indicating that this interaction

140   may not be essential. Conserved Lys259 is positioned to interact with an acidic patch on α-

141   tubulin formed by Asp424, Glu420, and Glu423. Ile260, conserved in hydrophobic character

142   across all R1 sequences, is buried within a hydrophobic pocket formed by α-tubulin residues

143   Ile265, Val435, and Tyr262 at the inter-dimer interface (Fig. 2C). Asn265, universally conserved

144   amongst repeats in classical MAPs (Fig. S5), forms a stabilizing intramolecular hydrogen bond

145   within the type II' β-turn formed by residues 263-266. Finally, Lys267 is positioned to interact

146   with the acidic α-tubulin C-terminal tail, and its basic character is conserved.

147   It was not possible to reliably model the peptide backbone beyond this 12-residue

148   stretch of the R1 tau density. We hypothesized that residues 242-255 lack ordered interactions

149   with tubulin. This region is rich in prolines in R1, in contrast to the distinct, conserved

150   hydrophobic pattern present in both R2 and R3 (Fig. 1A, S5). To further investigate whether the

151   repeats can form additional interactions with the MT surface, we next obtained a cryo-EM

152   reconstruction of a synthetic tau construct containing four copies of repeat R2 (R2x4) (overall

153   resolution of 3.9 Å) (Fig. 3A and S1C). Although the densities for R1x4 and R2x4 are similar at

154   the inter-dimer interface (Fig. 2 and S6A), the R2x4 reconstruction has additional tau density

155   along the surface of β-tubulin. We modeled a stretch of 27 backbone residues into the R2x4 tau

156   density, spanning three tubulin monomers and corresponding almost to a length of

157   approximately 80 Å, the length of a tubulin dimer repeat on the MT lattice. Using the same

158   Rosetta-guided modeling as with R1, we refined all possible tau sequence registers. As with R1,

159   we discovered a single, strongly preferred register and conformation for R2 (Fig. 3B) that was

160   similarly robust when modeling with a more computationally intensive sampling protocol.

161   Importantly, the solutions for R1 and R2 corresponded to the same sequence register. At

162   equivalent positions at the inter-dimer interface, the R1 and R2 atomic models are virtually

163   identical (Fig. 3C), with conserved residues sharing critical tau-tubulin contacts. For two non-

164   conserved positions, Cys291(R2) instead of Ile260(R1), and Lys294(R2) instead of Thr263(R1)

165   (Fig. 3C), the nature of the interactions are preserved (free cysteines demonstrate strong

166   hydrophobic character(*28*) and Lys294 likely interacts with the acidic C-terminal tail (Fig. 4)).

167   The robustness of this solution, with the same sequence register and atomic details from two

168   independent maps, provides very high confidence that our sequence assignments – and the

169   resulting atomic details – are correct. The consensus register of our atomic models for R1 and

170   R2 is further supported by previous gold-tagging results, which localized MAP2 Lys368 (Fig. S6)

171   to the H12 helix in tubulin at the interface between tubulin subunits(*14*). In our atomic model, the

172   equivalent Gln276 of R2 maps to the intra-dimer interface at the C-terminal end of helix H12 in

173   β-tubulin (Fig. S6), in excellent agreement with the labeling studies.

174   Additional residues in our R2x4 model include the peptide VQIINKK (not conserved in

175   R1), which had been previously shown to promote MT polymerization(*25*) and to bind

176   independently of the conserved sequence that targets the inter-dimer interface(*6*). This R2

177   peptide localizes to the intra-dimer interface and is sufficiently close to interact with the β-tubulin

178   C-terminal tail (Fig. 4B). Residues Val275, Ile277, Leu282 and Leu284 (Fig. 3D, 4B) are buried

179   against the MT-surface and tolerate only conservative hydrophobic substitutions in R2, R3 and

180   R4 (Fig. S5). As further support for our model, Lys274 and Lys281 of tau have previously been

181   shown to be crucial for tau-MT binding(*6*), and in our atomic model Lys274 is sufficiently close

182   to interact with an acidic patch on the MT-surface formed by Asp427 and Ser423 (Fig. 4A),

183   while Lys281 is well positioned to interact with the β-tubulin C-terminal tail (whereas Lys280,

184   which had little effect on tau affinity, is not) (Fig. 4A). Finally, the highly conserved His299 in R2

185   is buried in a cleft formed by β-tubulin residues Phe395 and Phe399 (Fig. 3C and Fig. 4A).

186   We observe that the major tau binding site between tubulin dimers localizes to the

187   previously defined 'anchor point', a tubulin region that remains unaltered during the structural

188   changes accompanying nucleotide hydrolysis within the MT, and even when comparing

189   assembled and disassembled states of tubulin(*16*). Indeed, superimposing the bent (4I4T(*29*))

190   and straight forms of tubulin (3JAR(*16*)) (Fig. 5, right) reveals that the tau-tubulin contacts at the

191   tubulin dimer interface are significantly preserved in the former. This finding agrees with and

192   explains the observation that tau added to tubulin under non-assembling conditions results in

193   the formation of tubulin rings(*30*), and with the co-purification of classical MAPs, including tau,

194   through temperature-driven tubulin assembly-disassembly cycles.

195   Although we could model most of the residues in a tau repeat, we could not clearly

196   visualize the highly conserved PGGG motif, which would correspond to the region connecting

197   the modeled segments. A prior study reported a β-turn structure for the PGGG motif(*13*).

198   However, the construct utilized in that study contained PGGG at the N- and C-termini, and it is

199   possible that the reported state is present only when there is no binding of PGGG-flanking

200   residues. Recent findings suggest that the PGGG motif may play a role when bound to

201   unassembled tubulin(*31*).

202   Tau is an important cellular factor required for specialized MT arrangements, and it has

203   been long debated how tau may cross-link MTs to form higher order structures. Our results

204   suggest that all four tau repeats are likely to associate with the MT surface in tandem through

205   adjacent tubulin subunits along a PF. This modular structure explains how alternatively spliced

206   variants (regulated developmentally or in disease states) can have essentially identical

207   interactions with tubulin but different affinity based on the number of repeats present. However,

208   if one or two of the repeats were used as "spacers", then tau would possibly be able to reach

209   across adjacent PFs, as previously proposed(*32, 33*), or even cross-link MTs, using its repeat

210   sequences. Additionally, other sequence elements distinct from the repeats, such as the

211   projection domain, could engage with tubulin to add tethering points with the MT surface, both

212   within and between MTs. Such additional interactions of tau would likely engage the

213   unstructured tubulin C-terminal tails, as otherwise we would likely have seen some difference

214   between our full-length and shorter tau construct reconstructions.

215

216   In summary, our MT-tau structures lead to a model in which each tau repeat spans both

217   intra- and inter-dimer interfaces, centered on α-tubulin and connecting three tubulin monomers.

218   In the context of full-length tau, repeats are likely to bind one after the other in tandem along a

219   PF, promoting MT polymerization and stabilization by tethering tubulin dimers together across

220 longitudinal interfaces (Fig. 5, left). Other structural elements could potentially be involved in

221 inter-PF or inter-MT interactions. Regardless of the construct used, we observe an extended

222 conformation for the MT-binding repeat. The details of the repeat structure and MT interactions

223 are supported by our extensive modeling on two independently determined reconstructions, and

224 account for previous biochemical and structural observations. However, a number of important

225 questions remain open concerning the range of configurations of full-length tau-MT binding

226 under physiological, non-saturating conditions. The strikingly conserved PGGG motif is not

227 visible in any of our reconstructions and its structural role remains unsolved. It is possible that

228 the flexibility of this motif is needed to allow binding to the different conformational states of

229 tubulin in oligomers and MTs. Alternatively, the PGGG motif may play a critical role in

230 association of tau with substrates other than tubulin, such as actin(*34*).

231

232

233 **References and Notes**:

234 1.   C. Conde, A. Caceres, Microtubule assembly, organization and dynamics in
235   axons and dendrites. *Nat Rev Neurosci* **10**, 319-332 (2009).
236 2.   K. S. Kosik, L. D. Orecchio, S. Bakalis, R. L. Neve, Developmentally regulated
237   expression of specific tau sequences. *Neuron* **2**, 1389-1397 (1989).
238 3.   A. Himmler, D. Drechsel, M. W. Kirschner, D. W. Martin, Jr., Tau consists of a set
239   of proteins with repeated C-terminal microtubule-binding domains and variable N-
240   terminal domains. *Mol Cell Biol* **9**, 1381-1388 (1989).
241 4.   D. J. Ennulat, R. K. Liem, G. A. Hashim, M. L. Shelanski, Two separate 18-amino
242   acid domains of tau promote the polymerization of tubulin. *J Biol Chem* **264**,
243   5327-5330 (1989).
244 5.   K. A. Butner, M. W. Kirschner, Tau protein binds to microtubules through a
245   flexible array of distributed weak sites. *J Cell Biol* **115**, 717-730 (1991).
246 6.   B. L. Goode, S. C. Feinstein, Identification of a novel microtubule binding and
247   assembly domain in the developmentally regulated inter-repeat region of tau. *J
248   Cell Biol* **124**, 769-782 (1994).
249 7.   A. C. Alonso, T. Zaidi, I. Grundke-Iqbal, K. Iqbal, Role of abnormally
250   phosphorylated tau in the breakdown of microtubules in Alzheimer disease. *Proc
251   Natl Acad Sci U S A* **91**, 5562-5566 (1994).
252 8.   A. C. Alonso, I. Grundke-Iqbal, K. Iqbal, Alzheimer's disease
253   hyperphosphorylated tau sequesters normal tau into tangles of filaments and
254   disassembles microtubules. *Nat Med* **2**, 783-787 (1996).

255   9.   N. Gustke *et al.*, The Alzheimer-like phosphorylation of tau protein reduces
256   microtubule binding and involves Ser-Pro and Thr-Pro motifs. *FEBS Lett* **307**,
257   199-205 (1992).
258   10.   A. W. P. Fitzpatrick *et al.*, Cryo-EM structures of tau filaments from Alzheimer's
259   disease. *Nature* **547**, 185-190 (2017).
260   11.   D. Eliezer *et al.*, Residual structure in the repeat domain of tau: echoes of
261   microtubule binding and paired helical filament formation. *Biochemistry* **44**, 1026-
262   1036 (2005).
263   12.   X. H. Li, J. A. Culver, E. Rhoades, Tau Binds to Multiple Tubulin Dimers with
264   Helical Structure. *J Am Chem Soc* **137**, 9218-9221 (2015).
265   13.   H. Kadavath *et al.*, Folding of the Tau Protein on Microtubules. *Angew Chem Int
266   Ed Engl* **54**, 10347-10351 (2015).
267   14.   J. Al-Bassam, R. S. Ozer, D. Safer, S. Halpain, R. A. Milligan, MAP2 and tau
268   bind longitudinally along the outer ridges of microtubule protofilaments. *J Cell
269   Biol* **157**, 1187-1196 (2002).
270   15.   S. Kar, J. Fan, M. J. Smith, M. Goedert, L. A. Amos, Repeat motifs of tau bind to
271   the insides of microtubules in the absence of taxol. *EMBO J* **22**, 70-77 (2003).
272   16.   R. Zhang, G. M. Alushin, A. Brown, E. Nogales, Mechanistic Origin of
273   Microtubule Dynamic Instability and Its Modulation by EB Proteins. *Cell* **162**, 849-
274   859 (2015).
275   17.   R. Zhang, E. Nogales, A new protocol to accurately determine microtubule lattice
276   seam location. *J Struct Biol* **192**, 245-254 (2015).
277   18.   G. M. Alushin *et al.*, High-resolution microtubule structures reveal the structural
278   transitions in alphabeta-tubulin upon GTP hydrolysis. *Cell* **157**, 1117-1129
279   (2014).
280   19.   M. F. Chau *et al.*, The microtubule-associated protein tau cross-links to two
281   distinct sites on each alpha and beta tubulin monomer via separate domains.
282   *Biochemistry* **37**, 17692-17703 (1998).
283   20.   L. Serrano, E. Montejo de Garcini, M. A. Hernandez, J. Avila, Localization of the
284   tubulin binding site for tau protein. *Eur J Biochem* **153**, 595-600 (1985).
285   21.   H. Kadavath *et al.*, Tau stabilizes microtubules by binding at the interface
286   between tubulin heterodimers. *Proc Natl Acad Sci U S A* **112**, 7501-7506 (2015).
287   22.   B. Trinczek, A. Ebneth, E. M. Mandelkow, E. Mandelkow, Tau regulates the
288   attachment/detachment but not the speed of motors in microtubule-dependent
289   transport of single vesicles and organelles. *J Cell Sci* **112 (Pt 14)**, 2355-2367
290   (1999).
291   23.   Y. Song *et al.*, High-resolution comparative modeling with RosettaCM. *Structure*
292   **21**, 1735-1742 (2013).
293   24.   R. Y. Wang *et al.*, Automated structure refinement of macromolecular assemblies
294   from cryo-EM maps using Rosetta. *Elife* **5**, (2016).
295   25.   D. Panda, B. L. Goode, S. C. Feinstein, L. Wilson, Kinetic stabilization of
296   microtubule dynamics at steady state by tau and microtubule-binding domains of
297   tau. *Biochemistry* **34**, 11117-11127 (1995).
298   26.   J. Biernat, N. Gustke, G. Drewes, E. M. Mandelkow, E. Mandelkow,
299   Phosphorylation of Ser262 strongly reduces binding of tau to microtubules:

300   distinction between PHF-like immunoreactivity and microtubule binding. *Neuron*
301   **11**, 153-163 (1993).

302 27.   M. Hasegawa *et al.*, Protein sequence and mass spectrometric analyses of tau in
303   the Alzheimer's disease brain. *J Biol Chem* **267**, 17047-17054 (1992).

304 28.   N. Nagano, M. Ota, K. Nishikawa, Strong hydrophobic nature of cysteine
305   residues in proteins. *FEBS Lett* **458**, 69-71 (1999).

306 29.   A. E. Prota *et al.*, Molecular mechanism of action of microtubule-stabilizing
307   anticancer agents. *Science* **339**, 587-590 (2013).

308 30.   F. Devred *et al.*, Tau induces ring and microtubule formation from alphabeta-
309   tubulin dimers under nonassembly conditions. *Biochemistry* **43**, 10520-10531
310   (2004).

311 31.   S. Elbaum-Garfinkle, G. Cobb, J. T. Compton, X. H. Li, E. Rhoades, Tau mutants
312   bind tubulin heterodimers with enhanced affinity. *Proc Natl Acad Sci U S A* **111**,
313   6311-6316 (2014).

314 32.   R. A. Santarella *et al.*, Surface-decoration of microtubules by human tau. *J Mol*
315   *Biol* **339**, 539-553 (2004).

316 33.   A. R. Duan *et al.*, Interactions between Tau and Different Conformations of
317   Tubulin: Implications for Tau Function and Mechanism. *J Mol Biol* **429**, 1424-
318   1438 (2017).

319 34.   A. Elie *et al.*, Tau co-organizes dynamic microtubule and actin networks. *Sci Rep*
320   **5**, 9964 (2015).

321 35.   A. Tennstaedt *et al.*, Human high temperature requirement serine protease A1
322   (HTRA1) degrades tau protein aggregates. *J Biol Chem* **287**, 20931-20941
323   (2012).

324 36.   E. H. Kellogg *et al.*, Insights into the Distinct Mechanisms of Action of Taxane
325   and Non-Taxane Microtubule Stabilizers from Cryo-EM Structures. *J Mol Biol*
326   **429**, 633-646 (2017).

327 37.   B. Carragher *et al.*, Leginon: an automated system for acquisition of images from
328   vitreous ice specimens. *J Struct Biol* **132**, 33-45 (2000).

329 38.   X. Li *et al.*, Electron counting and beam-induced motion correction enable near-
330   atomic-resolution single-particle cryo-EM. *Nat Methods* **10**, 584-590 (2013).

331 39.   A. Rohou, N. Grigorieff, CTFFIND4: Fast and accurate defocus estimation from
332   electron micrographs. *J Struct Biol* **192**, 216-221 (2015).

333 40.   G. Tang *et al.*, EMAN2: an extensible image processing suite for electron
334   microscopy. *J Struct Biol* **157**, 38-46 (2007).

335 41.   N. Grigorieff, FREALIGN: high-resolution refinement of single particle structures.
336   *J Struct Biol* **157**, 117-125 (2007).

337 42.   E. H. Egelman, A robust algorithm for the reconstruction of helical filaments using
338   single-particle methods. *Ultramicroscopy* **85**, 225-234 (2000).

339 43.   D. N. Mastronarde, Automated electron microscope tomography using robust
340   prediction of specimen movements. *J Struct Biol* **152**, 36-51 (2005).

341 44.   S. Q. Zheng *et al.*, MotionCor2: anisotropic correction of beam-induced motion
342   for improved cryo-electron microscopy. *Nat Methods* **14**, 331-332 (2017).

343 45.   P. Emsley, B. Lohkamp, W. G. Scott, K. Cowtan, Features and development of
344   Coot. *Acta Crystallogr. D. Biol. Crystallogr.* **66**, 486-501 (2010).

345   46.   L. Holm, C. Sander, Database algorithm for generating protein backbone and
346   side-chain co-ordinates from a C alpha trace application to model building and
347   detection of co-ordinate errors. *J Mol Biol* **218**, 183-194 (1991).
348   47.   H. Park *et al.*, Simultaneous Optimization of Biomolecular Energy Functions on
349   Features from Small Molecules and Macromolecules. *J Chem Theory Comput*
350   **12**, 6201-6212 (2016).
351   48.   B. Gigant *et al.*, Structure of a kinesin-tubulin complex and implications for
352   kinesin motility. *Nat Struct Mol Biol* **20**, 1001-1007 (2013).
353

Acknowledgements:

368   **List of Supplementary Materials:**

369   **Materials and Methods**

370   **Figures S1-S6**

371   **Table S1**

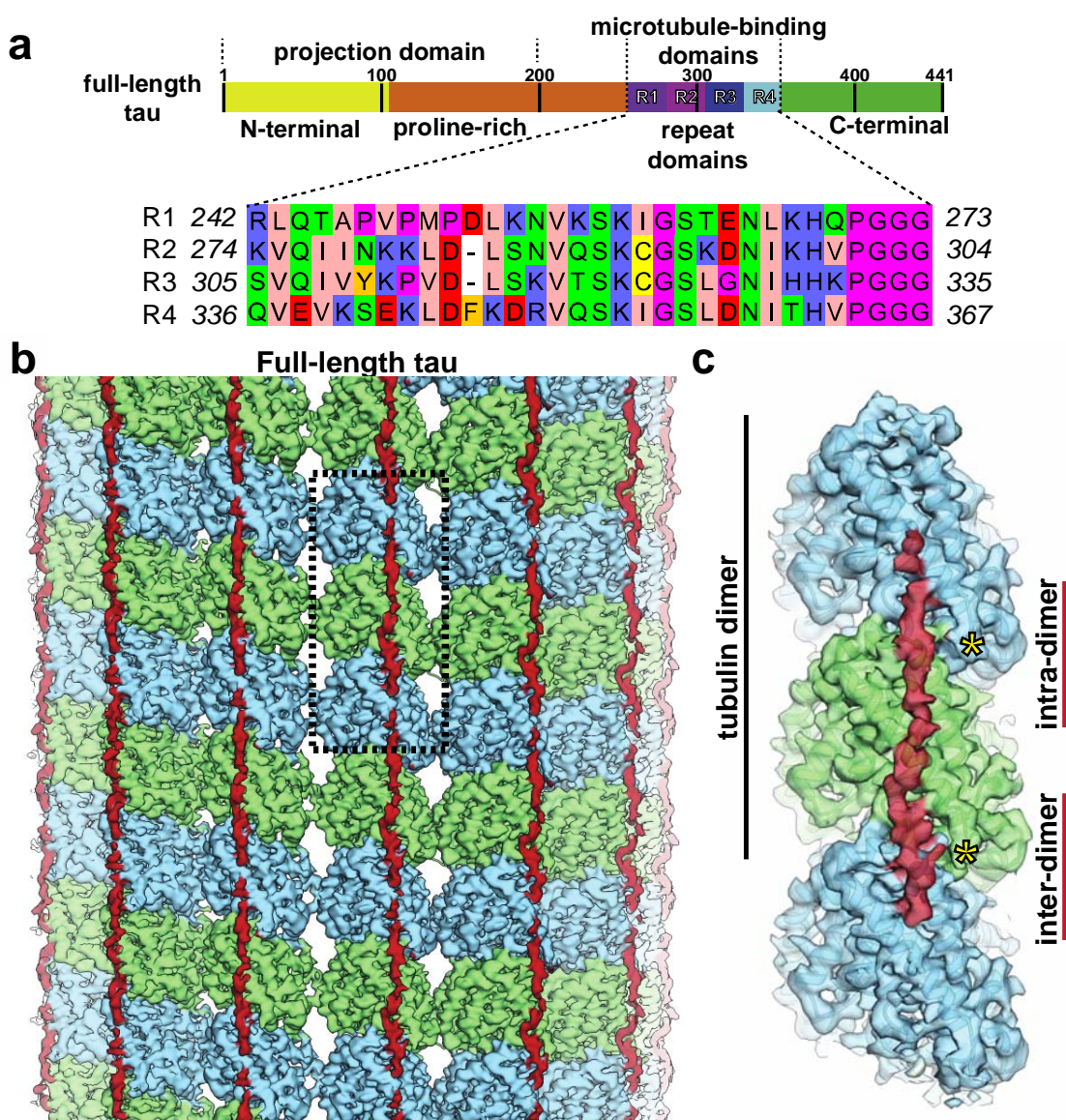372   **References (35-48)**

373

374

Fig. 1. Tau binding to microtubules. (A) Schematic of tau domain architecture and assigned functions. The MT-binding domain of four repeats includes residues 242-367. Inset shows the sequence alignment of the four repeat sequences, R1-4, that make up the repeat domain **(B)** Cryo-EM density map (4.1 Å overall resolution) of a MT decorated with full-length tau. Tau (red) appears as a nearly continuous stretch of density along PFs (α-tubulin in green, β-tubulin in blue). **(C)** The footprint of a continuous stretch of tau spans over three tubulin monomers, binding both across intra- and inter-dimer tubulin interfaces (only one repeat of tau is shown for clarity). Position of the C-termini of tubulin indicated with yellow asterisks.
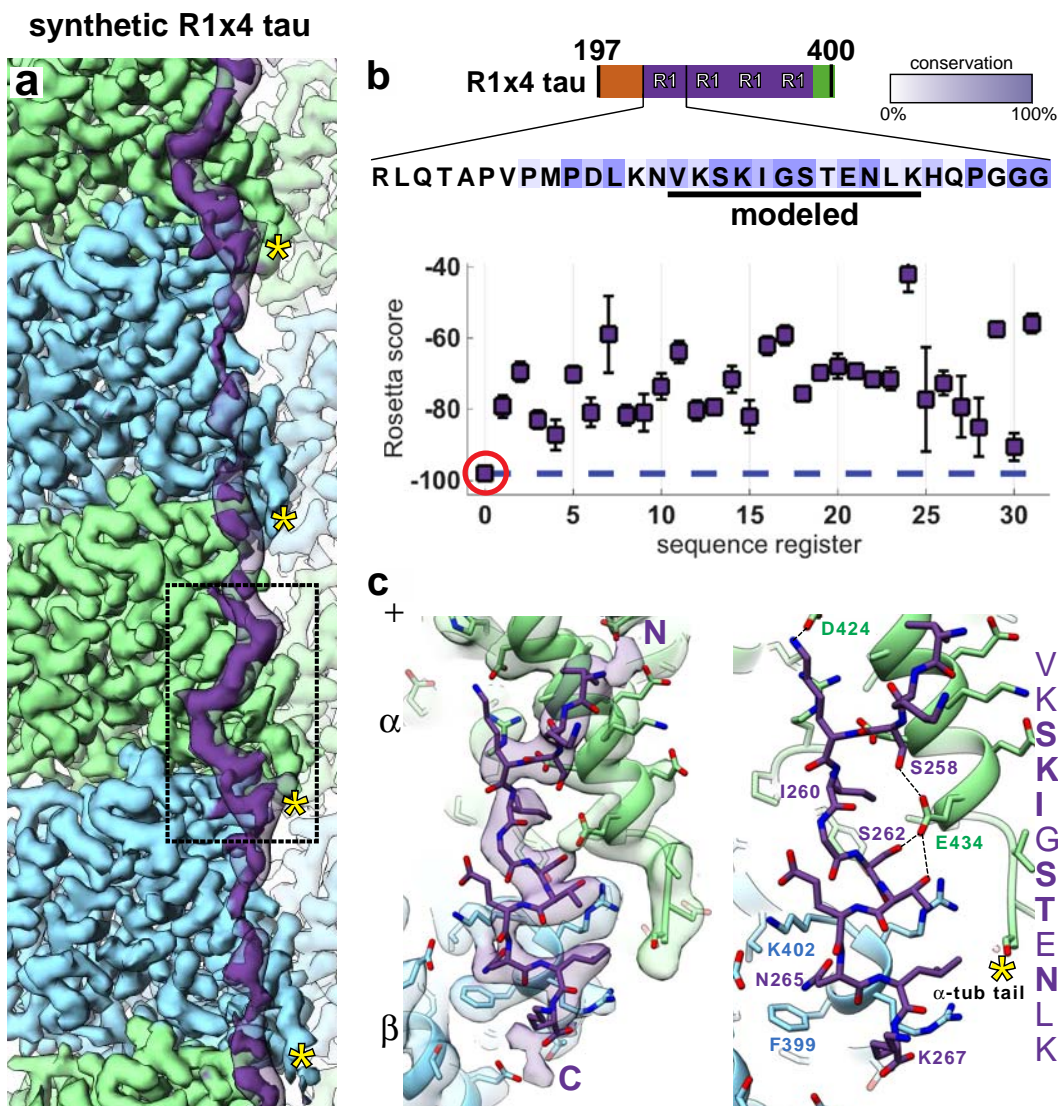
15

Fig. 2. Near-atomic resolution reconstruction of synthetic R1x4 tau on microtubules. (A) In the 3.2 Å cryo-EM reconstruction of tau-bound microtubules, the best-ordered segment of tau is bound at the interface between tubulin dimers (boxed) (lower threshold density for tau is shown in transparency). **(B)** Rosetta modeling reveals a single energetically preferred sequence register (red circle) for the best-ordered tau region, corresponding to a conserved (underlined) 12-residue stretch of residues within the R1 repeat sequence. Intensity of colored boxes indicates extent of conservation among tau homologs. **(C)** Atomic model of tau and tubulin, with (left) and without (right) the density map, showing the interactions over the inter-dimer region. C-termini of tubulin indicated with yellow asterisks in a and c.
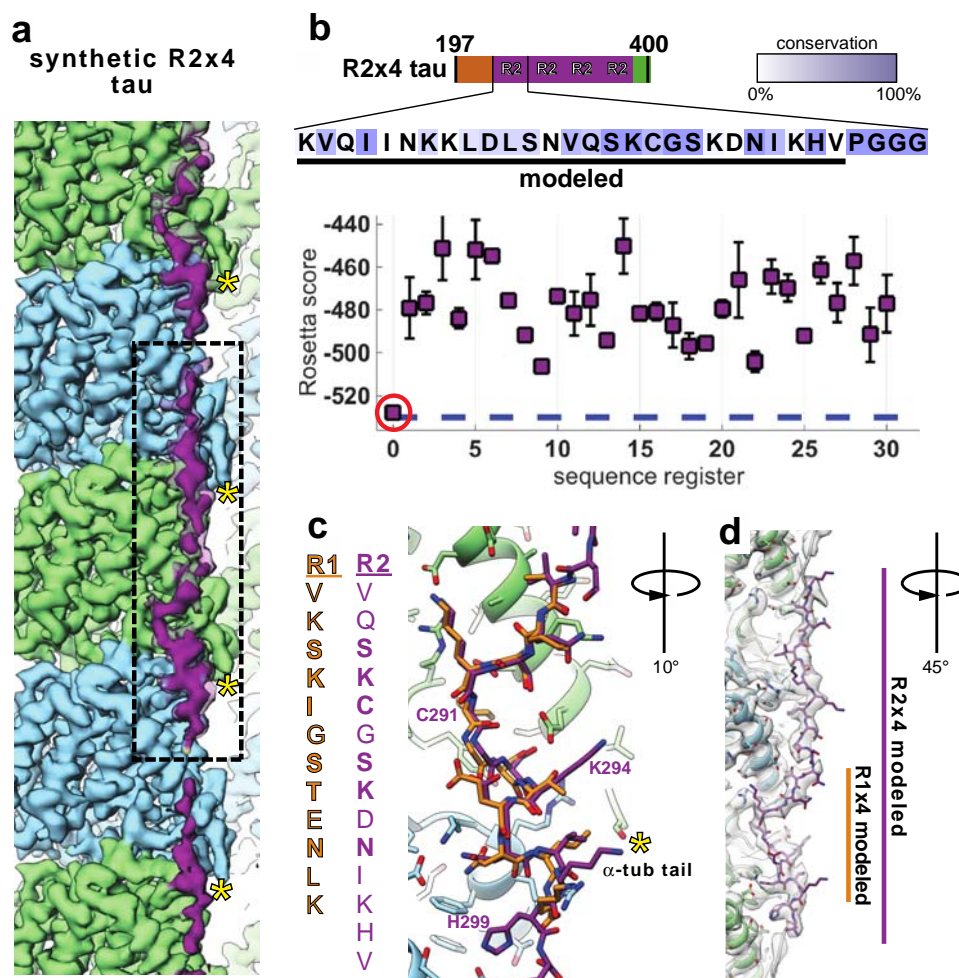
16

Fig. 3. High-resolution reconstruction of synthetic R2x4 tau on microtubules. (A) The (3.9 Å) cryo-EM reconstruction of R2x4 is highly similar to that of R1x4, but reveals a longer stretch of ordered density for tau along the MT surface (lower threshold density for tau is shown in transparency). **(B)** Rosetta modeling supports a sequence register (red circle) for the R2 sequence binding to tubulin analogous to that for R1 and shown in Fig. 2**. (C)** Major tau-tubulin interactions at the inter-dimer cleft are highly similar between the R1 (shown in goldenrod for easier visualization) and R2 (purple) sequences. **(D)** Extending the model to account for the additional density reveals an almost entire repeat of tau, spanning three tubulin monomers (centered on α-tubulin and contacting β-tubulin on either side) with an overall length of ~80 Å (the approximate length of a tubulin dimer). C-termini of tubulin indicated with yellow asterisks in a and c.
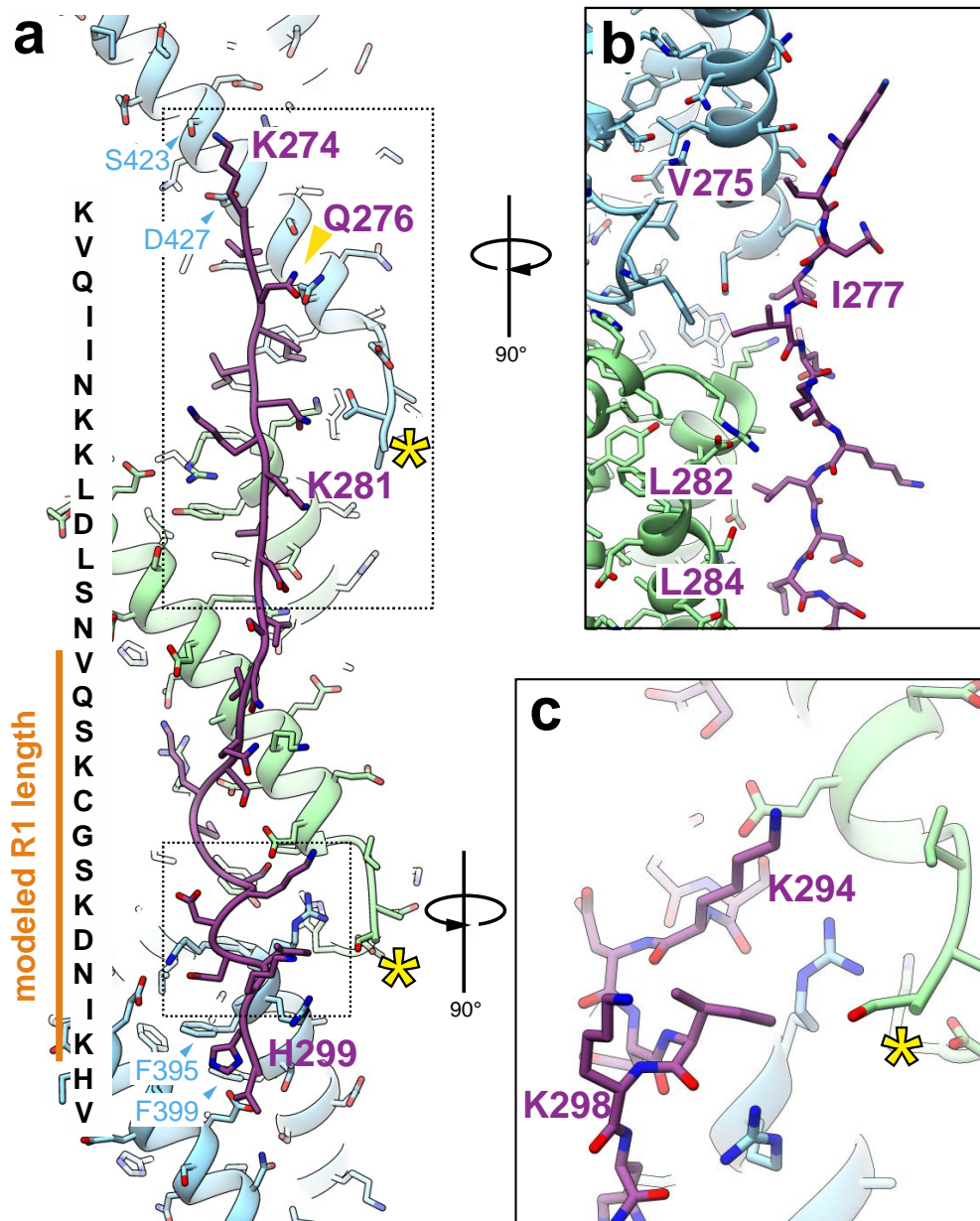
407
408 **Fig. 4. Repeat 2 makes additional conserved interactions with the MT surface. (A)** Atomic

409 model of the R2 repeat, shown along with the corresponding R2 sequence. The position of

410 previously studied gold-labeled tau(*14*) is indicated with a gold arrowhead (see also Fig. S6).

411 Boxed out regions show: **(B)** the hydrophobic packing of tau residues on the MT surface, and

412 **(C)** the positioning of two R2 lysines with potential interactions with the α-tubulin acidic C-

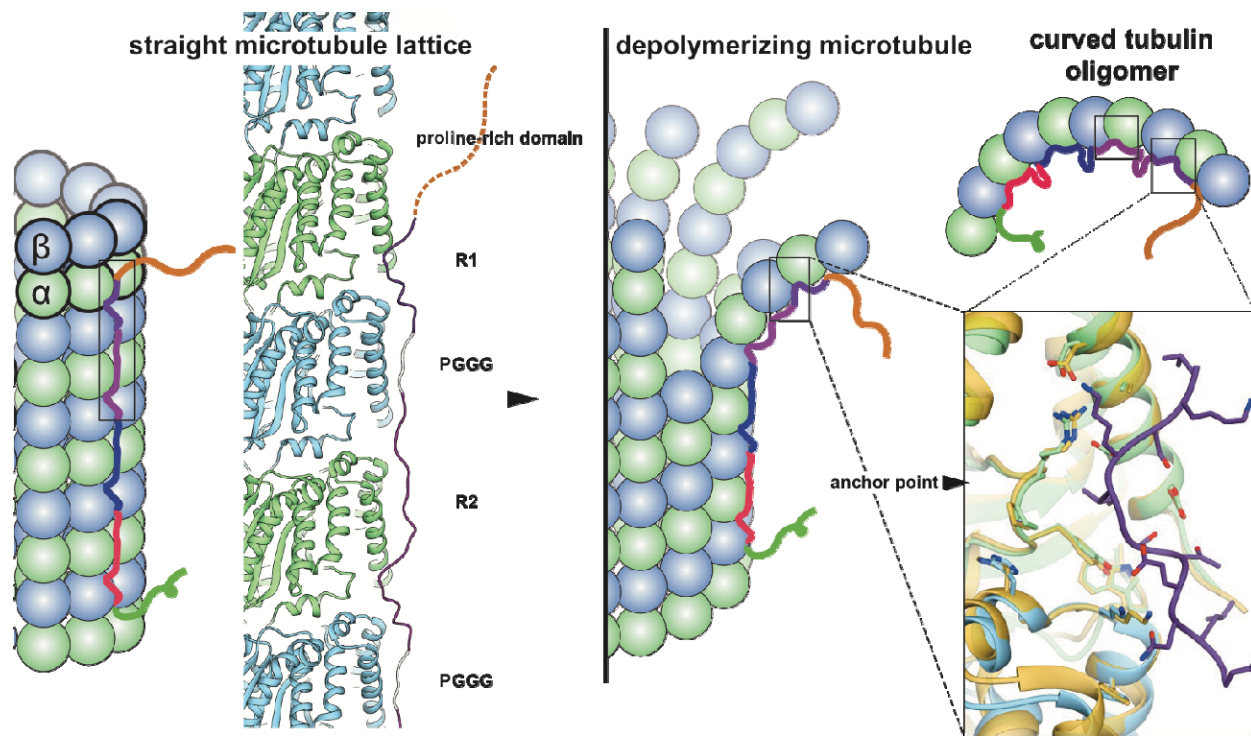413 terminal tail.

18

414
415
416 **Fig. 5. Model of full-length tau binding to microtubules and tubulin oligomers**. Our

417 structural data leads to a model of wild-type tau in which the four repeats bind in tandem along a

418 MT protofilament. Notice that we do not observe strong density for the region that would

419 correspond to the PGGG motif, which is modeled in gray for illustrative purposes and must be

420 highly flexible. Tau binding at the inter-dimer interface, interacting with both α- and β-tubulin,

421 promotes association between tubulin dimers. The tau binding site is also the location of the

422 previously identified "anchor point" (right-most box, gold is bent tubulin, PDB:4I4T (*29*) and

423 blue/green is straight tubulin, PDB: 3JAR (*16*)), and thus tau-tubulin interactions are unlikely to

424 change significantly with protofilament peeling during disassembly (center) or when bound to

425 small, curved tubulin oligomers (top-right).

426